Supplemental Information for

Pressure-tuned ideal P-type Schottky contacts

Zhaokuan Yu[1,2], Xuanyu Huang[2,3,4], Jinbo Bian[5], Yuqing He[2,3], Xin Lu[1,7,8,9], Quanshui Zheng[2,3,5,6*], Zhiping Xu[2,5*]

1) Department of Physics, Zhejiang University, Hangzhou 310027, China
2) Center for Nano and Micro Mechanics, Tsinghua University, Beijing 100084, China
3) State Key Laboratory of Tribology and Department of Mechanical Engineering, Tsinghua University, Beijing 100084, China
4) Department of Mechanical Engineering, Tsinghua University, Beijing 100084, China
5) Department of Engineering Mechanics, Tsinghua University, Beijing 100084, China
6) Institute of Superlubricity Technology, Research Institute of Tsinghua University in Shenzhen, Shenzhen 518057, China
7) Center of Correlated Matter, Zhejiang University, Hangzhou 310058, Zhejiang, China
8) Zhejiang Province Key Laboratory Quantum Technology and Device, Zhejiang University, Hangzhou 310027, Zhejiang, China
9) Collaborative Innovation Center of Advanced Microstructures, Nanjing University, Nanjing 210093, Jiangsu, China

[*]Corresponding authors: Z. Xu (xuzp@tsinghua.edu.cn) Q.-S. Zheng (zhengqs@tsinghua.edu.cn)

This Supplementary Information Material includes

Supplementary Notes S1-S15

Supplementary Figures S1-S15

Supplementary References

Content

S1. Fabrication of graphite mesa with Au films and MoS_2

To obtain graphite flakes, we first fabricated square graphite mesa arrays with an Au film on highly ordered pyrolytic graphite (HOPG, ZYB grade Brucker)[1]. In the fabrication process (Fig. S1), we first spun on a double-layer photoresist LOR 1A (100 nm)/ZEP (400 nm) on the fresh cleavage surface of the HOPG (i) and then removed the photoresist in the mesa array area by electron beam lithography (EBL) (ii). Secondly, we grew the Au array film with a thickness of 100 nm through electron beam evaporation (including the 10 nm Cr as an adhesion layer) (iii) and lift-off process (iv). Lastly, we used Au as a mask to obtain graphite mesa with an Au film by reactive ion etching (oxygen ions) (v), where the etching depth is 2.5 μm. Finally, we obtained the graphite mesa with an Au cap (vi).

For the fabrication of MoS_2, we first fabricated the Au film. We used electron beam evaporation to deposit a layer of 100 nm Au on one side of a 4-inch, 200 μm thick, double-polished silicon wafer with a crystalline surface, then used the wafer scriber to cut it into small pieces with sizes of 8 mm × 8 mm.

To remove impurities, the Au substrates were rinsed with acetone, isopropyl alcohol, and deionized water, heated at an elevated temperature of 150 °C for 20 min, and plasma-treated at 300 sccm and 500 W for 20 min. The working gas of the plasma treatment is 99.999%-pure O_2. We created devices from few-micron-sized MoS_2 flakes exfoliated from bulk 2H MoS_2 crystals (HQ Graphene) (Fig. S1b-i). We mechanically exfoliated MoS_2 sheets using the Scotch tape method and transferred them onto Au substrates under the ambient condition. Then the tape, with MoS_2 flakes adhered to it, was attached to the Au substrates and annealed at 150 °C for 20 min. Finally, the tape was peeled off, leaving a 10 nm-thick MoS_2 sheet on Au substrates. The whole procedure of sample preparation was finished in a clean room of Class 1000, with a temperature of ~25 °C and relative humidity of 30-60% (Fig. S1b-ii).

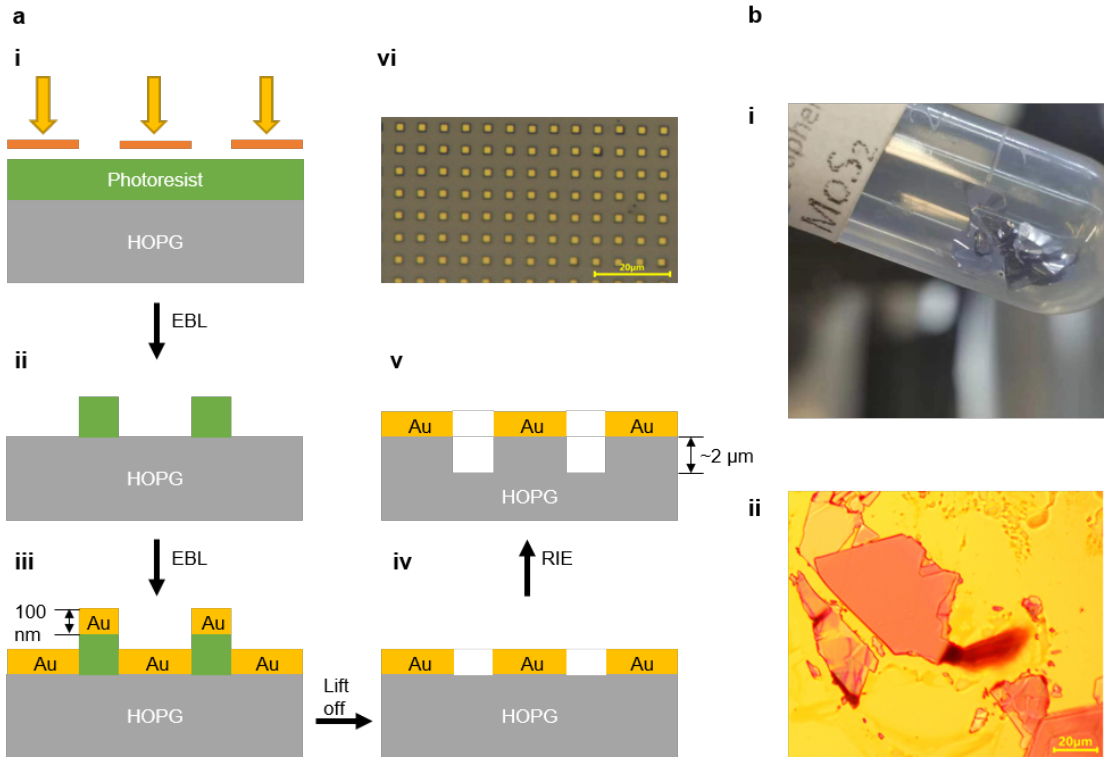

Fig. S1. Fabrication process of the graphite mesa with an Au cap and molybdenum disulfide (MoS_2) sheets on the Au film. (a, i-v) Flowchart of fabrication. (a, vi) Optical image of the fabricated graphite mesa with an Au cap. (b, i) MoS_2 single crystals. (b, ii) Cleavage of MoS_2 sheets on the Au film.

S2. The transfer process of graphite flakes

To form the SMG structure shown in Fig. 1a, we transferred graphite flake with a single crystal superlubric interface to the MoS_2 surface. The specific process is shown in Fig. S2, where the left side of each figure is the optical microscope (OM) observation, and the rest is the schematic diagram. Firstly, we used a tungsten micro-tip controlled by a micromanipulator (Kleindiek MM3A) to attach the Au cap of graphite mesa fabricated in Supplementary Note 1, as shown in Fig. S2a and applied shear stress by the micromanipulator until they split a short distance from their horizontal direction (Fig. S2b). Secondly, we removed the micro-tip to determine whether the sheared graphite flake undergoes self-retracting motion (SRM)[2] and whether there is a single-crystalline superlubric interface[3] (Fig. S2c). Lastly, we re-attached the graphite flake which has SRM properties with a micro-tip and split it out completely (Figs. S1d and e). We then removed

the dangling graphite flake dragged by the micro-tip and placed it slowly by micromanipulator on the atomically smooth fabricated MoS_2 (see Supplementary Note 1). At this time, since the adsorption of between the graphite flake and MoS_2 was stronger than that between the micro-tip and the graphite flake, the graphite flake would remain on the MoS_2 surface (Fig. S2f), forming the SMG structure shown in Fig. 1a. Since the interface of the finally transferred graphite flake was not exposed during the whole fabrication process in Supplementary Note 1, it would not be contaminated.

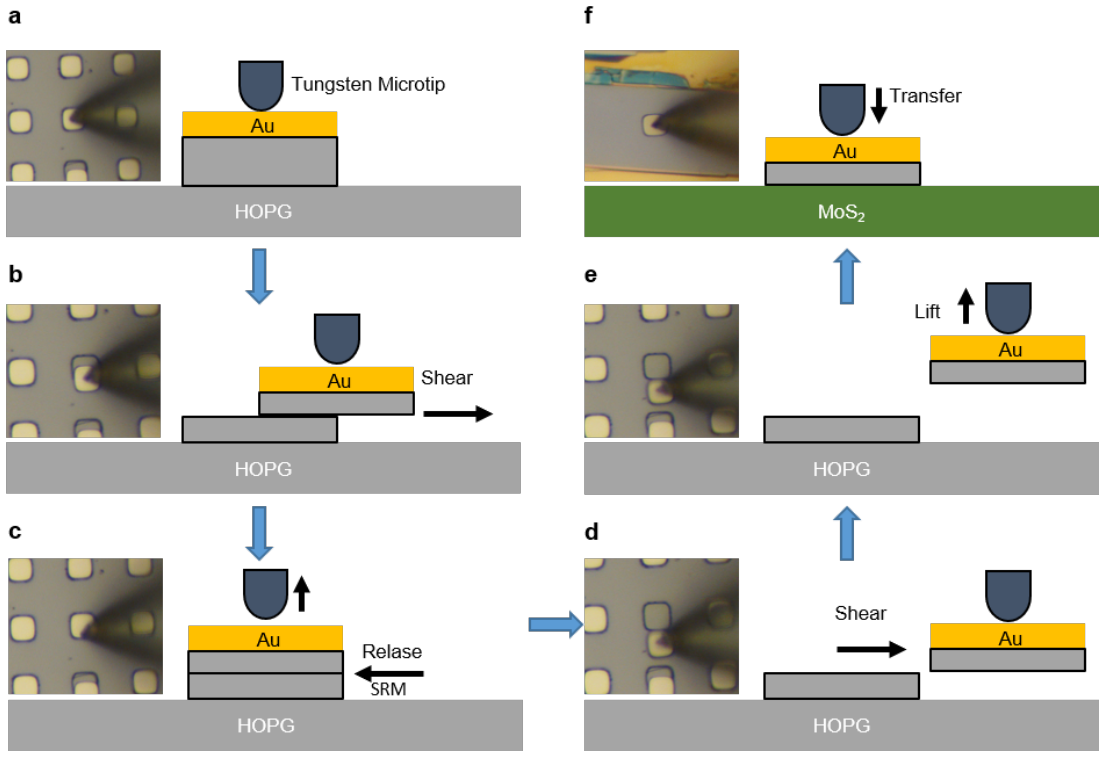

Fig. S2. Preparation of graphite flakes. (a) Attachment of the micro-tip and graphite mesa with Au cap. (b), (c) Observation of SRM. (d)-(f) Transfer process of graphite flake with SRM properties.

S3. Work function measurements of MoS_2 and HOPG

The work function of MoS_2 and HOPG were measured with the tip-coated Ir (ACCESS-NC-GG, Appnano) through an Asylum Research Cypher AFM in the scanning Kelvin probe microscope (SKPM) mode. The material parameters of measured MoS_2 were the same as with those chosen to produce Fig. 1a. The HOPG surface was obtained by shearing

cleavage. The results of the surface potentials of HOPG and MoS_2 were shown in Fig. S3a and b by scanning a smooth area, respectively. According to the working principle of SKPM, we could calculate the work function of HOPG (5.05 eV) and MoS_2 (5.12 eV).

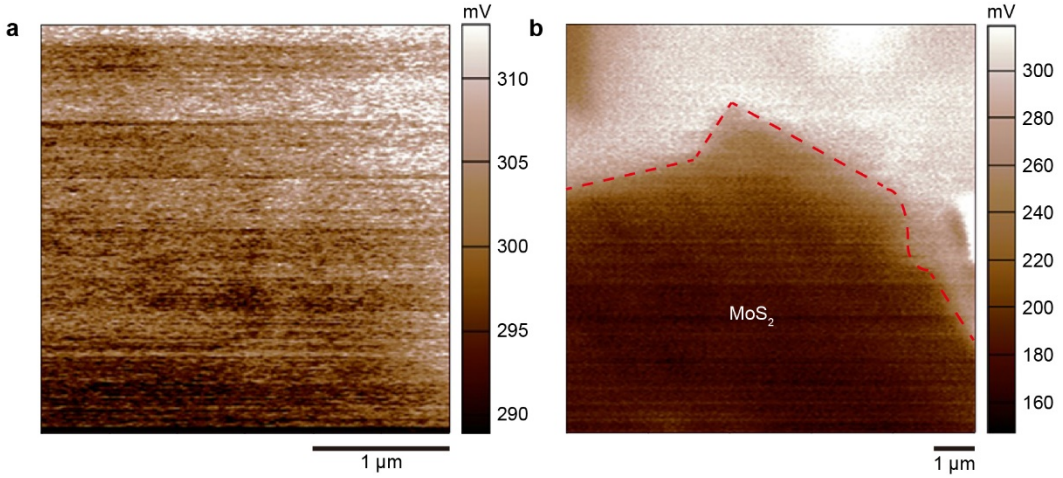

Fig. S3. SKPM measurements of HOPG and MoS_2 surfaces. (a) Surface potential between Ir AFM tip and HOPG. The work function of HOPG is $W_{Gr} = W_{Ir} - eV_s^{Gr}$ = (5.27-0.22) eV = 5.05 eV. (b) Surface potentials between Ir AFM tip and MoS_2.The work function of MoS_2 is $W_{MoS2} = W_{Ir} - eV_s^{MoS2}$ = (5.27 – 0.15) eV = 5.12 eV, respectively, where W_{Ir} is 5.27 eV is the work function of Ir.

S4. Friction and current measurements of the AFM system

The friction and current measurements of the graphite/MoS_2 junction were performed under an ambient atmosphere. The experimental set-up included a commercial NTEGRA upright AFM (NT-MDT), a 100 μm XYZ piezoelectric displacement platform, a high numerical aperture objective lens (×100 Mitutoyo) and a conductive AFM tip (ACCESS-NC-GG, Appnano). Fig. 1a shows the schematic of the experimental setup. We accurately pressed the AFM tip on the Au cap of the graphite flake through the OM and piezoelectric displacement platform. The AFM tip was calibrated *in-situ* by the Sader method[4,5] for the normal force and the diamagnetic levitation spring system[6] for the lateral force. The conductive AFM tip was grounded by connecting a precision ammeter, which can accurately measure the current through the AFM tip in the sliding process.

S5. Calibration of the AFM tips

Considering the friction measurement in Fig. 1c as an example, the normal force F_N was applied by the AFM cantilever, which can be written as $F_N=\alpha I/k$ where α is the optical lever sensitivity, k is the normal spring constant, and I is optical detector signal. The lever sensitivity was measured by performing a standard force curve measurement (Fig. S4a). We also obtained an average slope α = 0.0768 V/nm through the linear fitting. The normal spring constant k = 29.77 N/m was calibrated by the Sader method [4,5]. The optical detector signal I = 10 V was set by the AFM instrument. Therefore, we calculated the normal force of F = 32 μN.

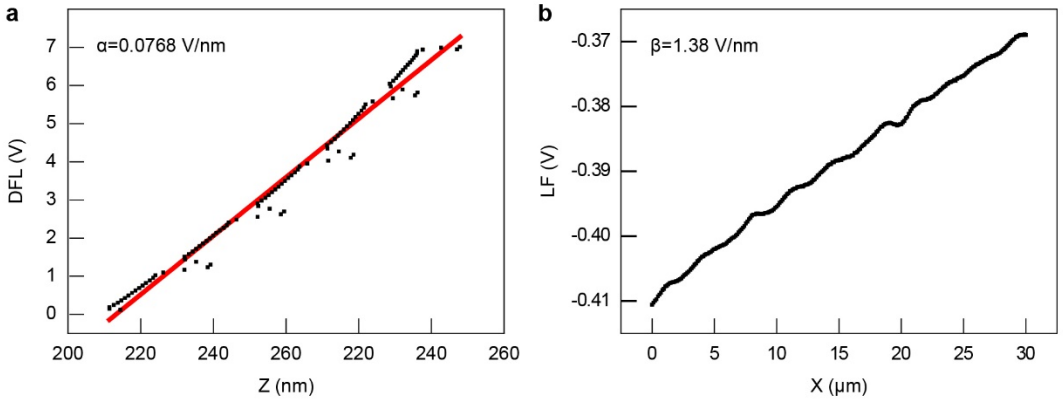

Fig. S4. Lever sensitivity measurements for normal and lateral calibration. (a) Standard force measurements for normal calibration. (b) Diamagnetic lateral force measurements for lateral calibration.

Similar to the normal force, the friction force f was measured by the AFM cantilever, which can be written as $f = (\beta I')/k'$ where β is the optical lever sensitivity, k' is the lateral spring constant of diamagnetic levitation system[6], and I' is measured frictional optical detector signal [6]. The k' = 3.05 x 10^{-2} N/m was calibrated by using the high-speed charge coupled device (CCD) to detect the vibration frequency of the levitate graphite sheet and precision balance to measure its mass[6]. The optical lever sensitivity was measured by using the AFM tip to drag the levitate graphite sheet and measure its force curve as shown in Fig. S4b, we tested 256 times, and one of them was drawn in the figure, and we obtained its average slope β = 1.38 V/nm through the linear fitting. Therefore, we calculated the lateral force coefficient $\gamma = \beta/k'$ = 39.45 nN/mV.

S6. Current noise measurements in the AFM system

To detect the current noise of the AFM (NT-MDT) current measurements, we adopted the same structure as in Fig. 1a, used the AFM tip static contact with the graphite flake, and the measured current noise I_{noise} is shown in Fig. S5a, where the x-axis is 256 data points collected in each cycle (the frequency is 1Hz), and the y-axis corresponds to the scanning line of each cycle. We further averaged the 256 data points of each cycle to obtain the relationship between the average current noise I_{noise} and time t (Fig. S5b). It can be seen that the noise in current was maintained at the order of 1 pA, which was much smaller than the measured current in Fig. 1c and illustrated the reliability of the measured current.

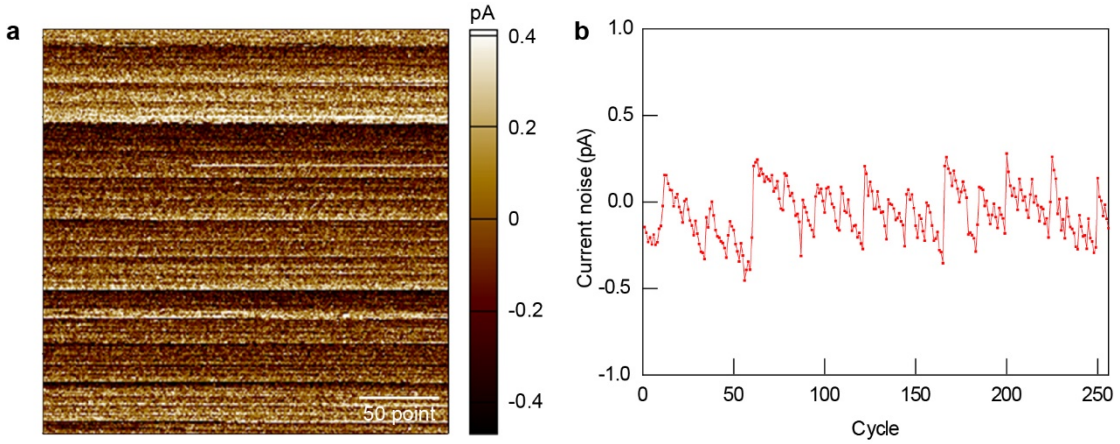

Fig. S5. Current noise measurements for AFM (NT-MDT) system. (a) Current noise I_{noise} map for 256 cycles (the frequency is 1Hz). Each cycle collects 256 data points. (b) Relationship between the average current noise I_{noise} and time t.

S7. Current-voltage characterization of the AFM system

To measure the I-V Curve *in-situ*, we used the applied voltage module of conductive AFM to measure the system. We first measured the bias voltage which is 9.7 mV of the C-AFM measurement system by a voltmeter. The voltage zeroing accuracy of the system was 0.1 mV, and the minimum step to change the voltage was 10 mV. After the current zeroing, the current noise can be lowered to 1 pA as shown in the Supplementary Note 6.

The voltage ranged from -0.5 V to 0.5 V and took 40 mV as a step. At the same time, we measured the current 10 s per step which can collect 5,120 data points to obtain more accurate measurements of the mean current. We also measured the I-V Curve under

different normal forces which range from 19.2 μN to 44.8 μN and step by 3.2 μN.

S8. Cypher AFM measurements of the critical pressure

To further assess our findings, we performed the critical pressure experiment on another AFM system of the Oxford Company models for Cypher. The experiment setup follows that in Fig.1a, and the measurements were carried out under the atmosphere. When the pressure reached 45 μN, the current suddenly rose from 0 pA to 40 pA (Fig. S6). At this point, we decreased the pressure by 1 μN, and the current immediately decreased to 0 pA. At the same time, this phenomenon can be repeated in the microscale manipulator system.

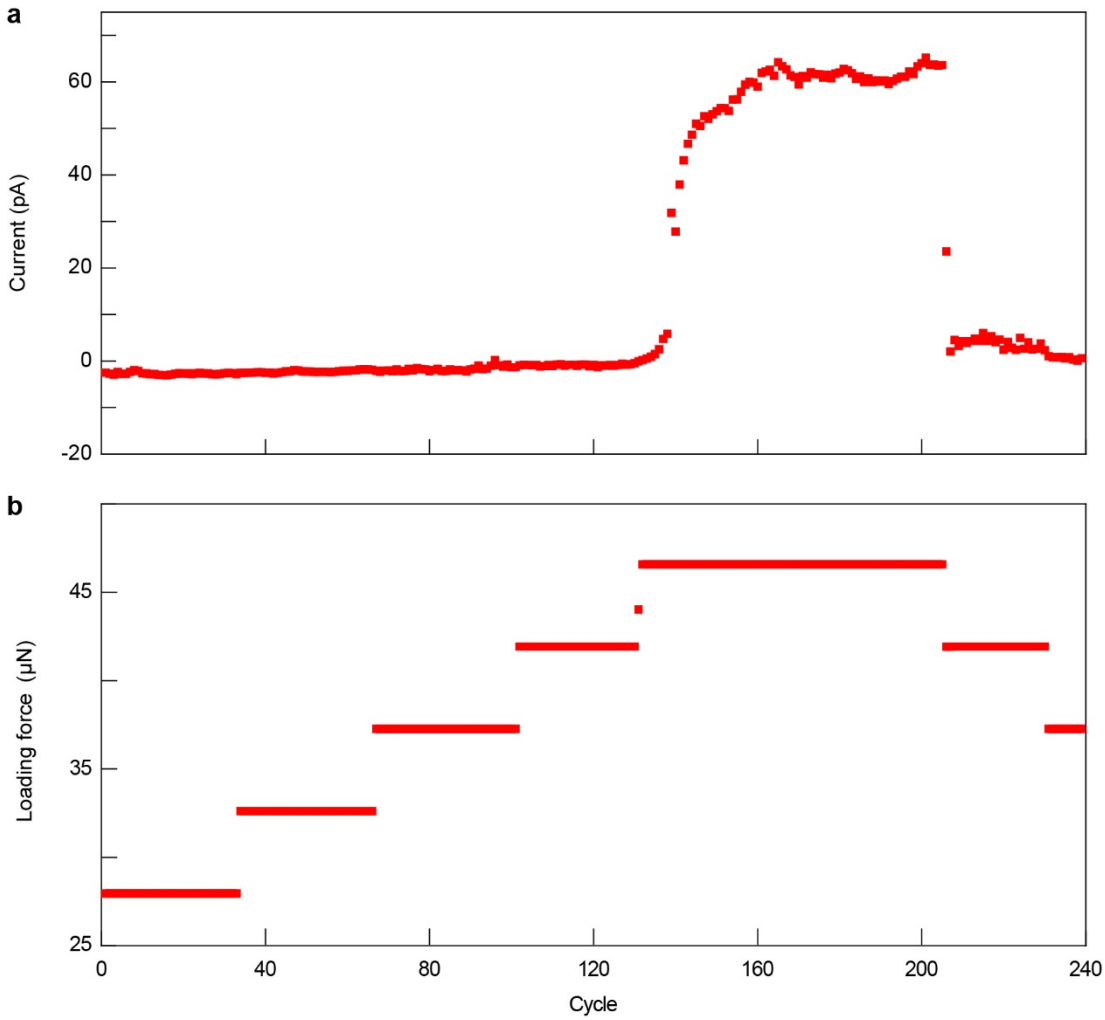

Fig. S6. Cypher AFM measurements of the critical pressure.

S9. Key parameters of SMGs for sensor applications

The application of SMG as a sensor showed excellent performance such as a response time of 30 ms, limit of detection of 4 MPa, lifespan of at least 120,000 cycles, sensitivity of 0.4 nA/kPa, and size in the order of 10 microns. We tested 512 points for each cycle. The measurement time at each point was about 2 ms. The response time was thus the difference between the moment when the current is stable and the moment when the current is zero, which is 30 ms (Fig. S7a). The sensitivity can be evaluated from the current difference divided by the pressure difference. The limit of detection is 4 MPa in our experiments shown in Fig.2a. The lifespan data is shown in Fig.1c, and the size is shown in Figs. 1b and 4a.

For the conversion efficiency of SMG, we measured the current and friction force simultaneously and loaded over the critical pressure (Fig. S7b). The current rose to 0.45 nA from zero and the friction force raised from 0.35 μN to 0.7 μN at the critical pressure. In this experiment, the amplitude was 2 μm and the frequency was 1 Hz. The open-circuit voltage was ~2 mV. Consequently, the conversion efficiency was calculated as the electrical power divided by the work done by friction, which is 50%. The conversion efficiencies measured in other samples are between 30% and 50%.

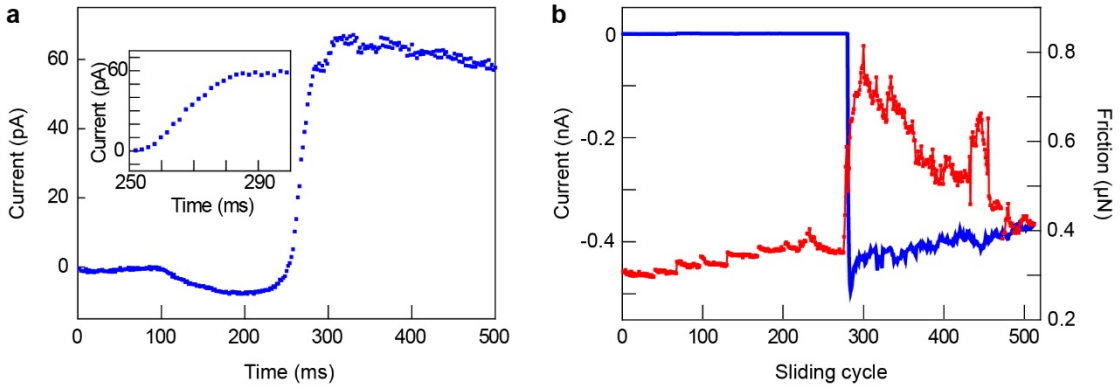

Fig. S7. Response time and conversion efficiency of SMG. (a) The response time is the difference between the moment when the current is stable and the moment when the current is zero, which is 30 ms. (b) The conversion efficiency is 50%, which is calculated at the moment the current increased to 0.45 nA from zero as the electrical power divided by the work done by friction.

S10. Current-voltage measurements of the microscale manipulator system

To accurately measure I-V curves, we used the applied voltage module of the Keithley 2410 voltmeter and a manipulator. The front end of the manipulator was connected with a tungsten tip of diameter 1 μm. The voltage was tuned from -1 V to 1 V with a step size of 10 mV. At the same time, we measured the current. We also measured I-V curves under different normal forces which range from 100 μN to 500 μN and step by 10 μN.

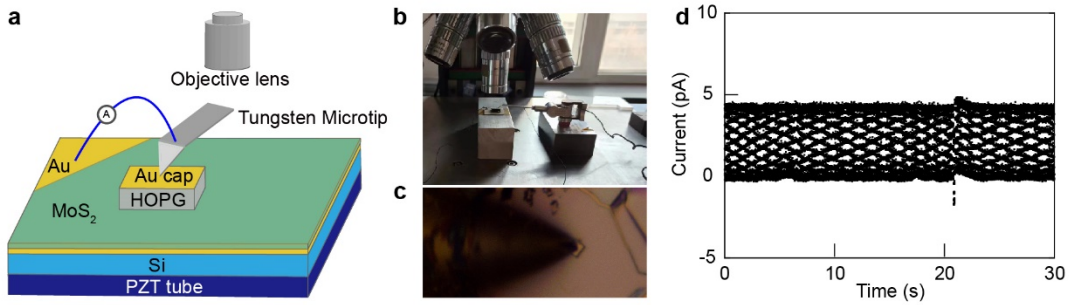

Fig. S8. Current-voltage measurements of SMG using the microscale manipulator system. (a) Structures of the microscale manipulator system. (b) Photography of the experimental setup. (c) Optical microscope (OM) observation. (d) Current noise I_{noise} of Keithley 2410 with a loading force of F_N = 250 μN as the function of time t.

To verify the Schottky contact formed by the graphite flake and MoS_2 and explain the strong normal force correlation in Fig. 2b, we used the system shown in Fig. S8, and measured the I-V curves under different normal forces (Fig. S9a). The positive direction of the bias voltage V was applied to the graphite flake relative to MoS_2, and the scan speed was 0.01 V/s. The unidirectional conduction characteristic showed that a Schottky junction was formed between the graphite flake and p-MoS_2 ($W_{MoS2} > W_{Gr}$), in which the forward conductivity was better for larger normal force. Subsequently, we used the thermionic emission model

$$I = AST^2 \exp\left(-\frac{\varphi}{k_B T}\right) \exp\left[\frac{e(V-IR_A)}{nk_B T}\right]\left[1-\exp\left(-\frac{e(V-IR_A)}{k_B T}\right)\right] \quad (1)$$

of the system by considering an additional resistance R_A to fit the ideal factor n and the Schottky barrier height φ corresponding to the measured data points, where A = 252 A/cm^2 is the effective Richardson constant, S =16 μm^2 is the contact area, e is the electron charge, k_B is Boltzmann constant, T = 283.15 K is the temperature.

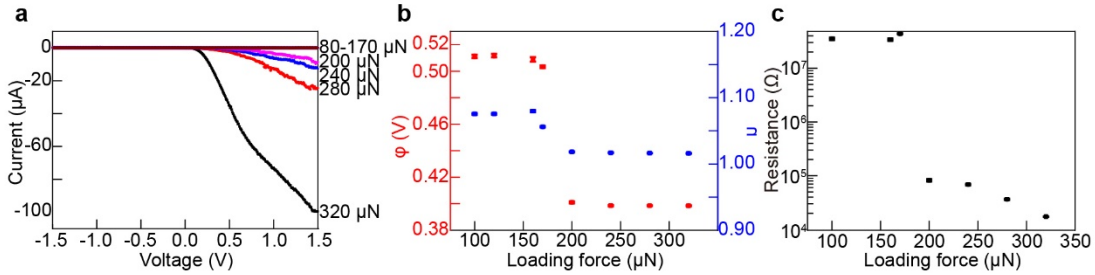

Fig. S9. Current-voltage measurements and fitting results for SMG. (a) Current-voltage measurement under different loading forces. (b) Fitting parameters of the Schottky barrier height and the ideal factor. (c) Fitting parameters of additional resistance.

We first focus on the inverse part ($V < 0$), the current $|I|$ is very small, that is, $|IR_A| \ll |V|$, Eq. (5) can be simplified to

$$I^* = AST^2 \exp\left(-\frac{\varphi}{k_B T}\right) \exp\left(\frac{eV}{nk_B T}\right) \quad (2)$$

Where $I^* = I[1\text{-}\exp(-eV/(k_B T))]^{-1}$ is the effective current, which showed exponential relationship (the linear relationship is shown in a semi-logarithmic graph). The fitted ideal factor n and Schottky barrier height φ under different normal forces by Eq. (2) are shown in Fig. S9b. The φ and n showed the same normal force dependence with AFM measurements.

On the contrary, when $V > 1$ V $>> k_B T/e$, the Eq. (5) can be simplified to

$$V = \frac{nk_B T}{e} \log\left(\frac{I}{SAT^2} \exp\left(\frac{\varphi}{k_B T}\right)\right) + IR_A \quad (3)$$

The values of fitted n and φ obtained in Fig. S9b could be substituted into Eq. (3), and the measured data points of $V > 1$ V could be used to fit the additional resistance R_A under different normal forces (Fig. S9c), which shows a decreasing trend and the critical point as the normal force increases.

S11. Current generation in the microscale manipulator system

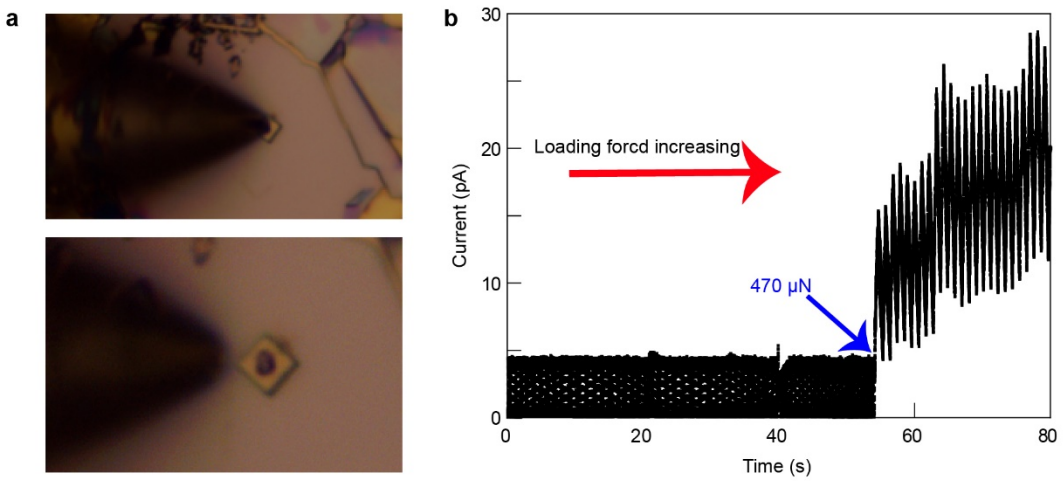

Fig. S10. (a) OM observation of SMGs and damage under larger forces. (b) The current measurements of SMGs with increasing pressure increase, the current emerges at the force F_N = 470 μN.

To verify the critical pressure for current generating formed by the graphite flake and MoS_2, we used the same system as shown in Fig. S8 and replaced the voltmeter with the Keithley 6514 electrometer in the atmosphere condition. As the pressure reaches 470 μN, the current suddenly rises from 0 pA to 15 pA (Fig. S10). At the same time, this phenomenon can be repeated in two types of AFM systems.

S12. Surface characterization in tribological experiments

In order to verify the contact between the graphite flakes and MoS_2 in the SMG is in the state of structural superlubricity (SSL), we conducted a series of tribological tests as shown in Fig 4.1. Here, we showed the specific process and method of the experiment. The first step was to characterize the two sliding surfaces, for the graphite flake surface, we used the method described in Supplementary Note 2 to select graphite flake with SRM properties (Fig. S2). We used Asylum Research Cypher AFM in the tapping mode to characterize the topography of surface for MoS_2 (Fig. 1b). For the second step, we used the lateral force measurement system of AFM (NT-MDT) to measure the relationship between friction force and normal force with displacement amplitude of 2 μm and speed of 4 μm/s, where each point was tested 50 times. Then we fitted the corresponding friction coefficient (Fig. 4b) and measured the friction force of 140,000 cycles sliding process under a normal force of 45 μN (Fig. 1c). For the third step, we performed some characterizations on the two surfaces after 140,000 sliding cycles. For the slid MoS_2 surface, we firstly used the Asylum

Research Cypher AFM in the tapping mode to perform morphological characterization over a wider area of 20 × 20 μm and found the positions of the graphite flake (Fig. S11), that is, located the sliding region (the yellow dashed frame). And we further characterized the small sliding region of MoS_2 through the positioning function of AFM to judge whether there is any observable damage on the slid MoS_2 surface (Fig. 4a).

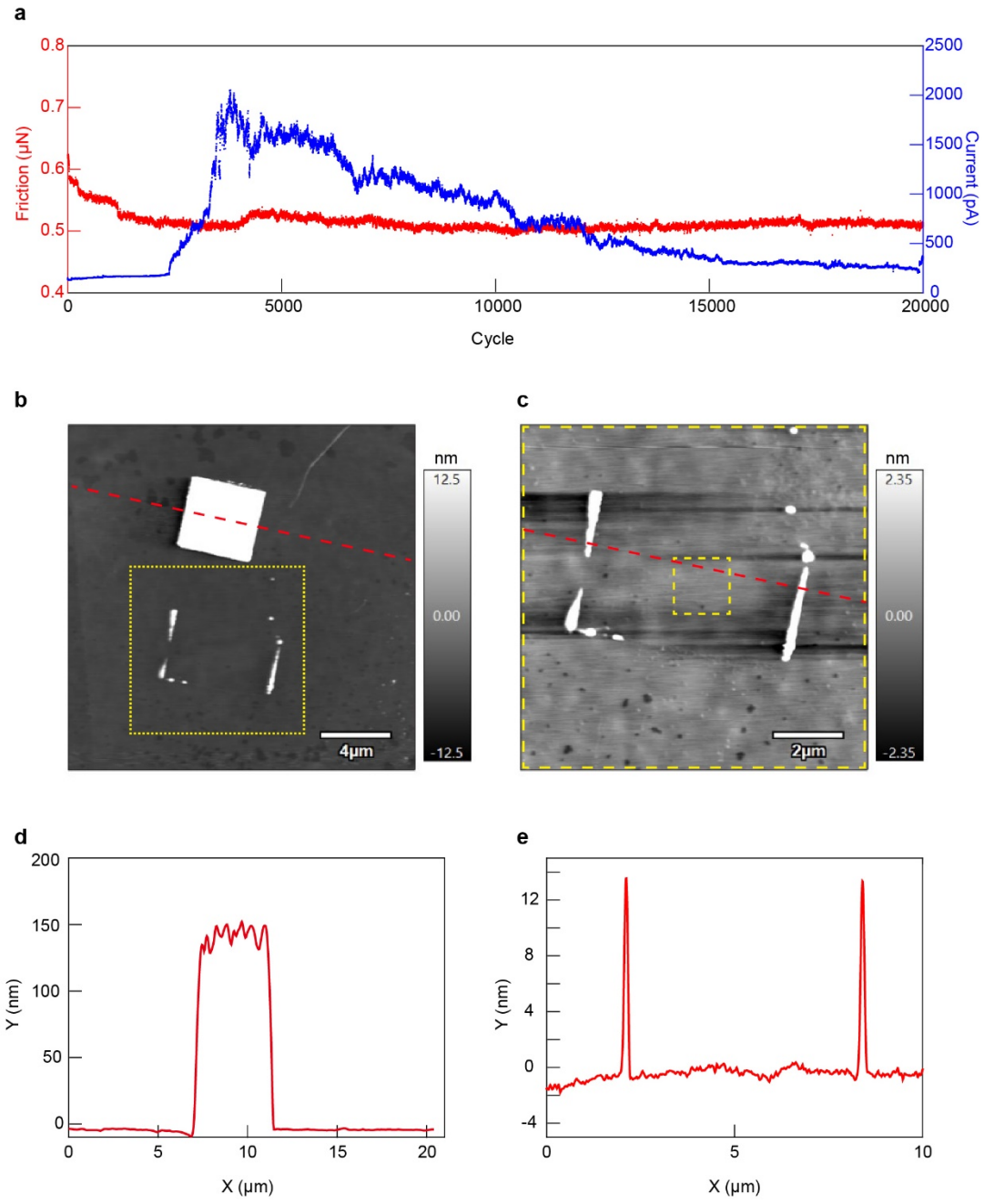

Fig. S11. Morphological characterization of the graphite flake and slid MoS_2 surfaces. (a)

The current and friction measurements of the running-in process for the first 20,000 cycles. (b, d) Morphological characterization of the graphite flake and slid MoS_2 surfaces and the red dash line is the height of graphite. (c, e) Zoom-in view of the yellow zone (in panel b) for the morphological characterization of the slid MoS_2 surface and the red dash line is the height of the MoS_2 surface.

For the fourth step, we performed Raman mapping characterization (LabRAM HR Evolution Raman spectrometer, Horiba) on the slid MoS_2 surface with a resolution of 0.1 cm^{-1}, laser wavelength of 532 nm, grating of 1800 (450-850 nm) acquisitions. Time of 4 s and spot diameter of 1 μm. The intensity distribution of the G peak (1580 cm^{-1}) in the range of 10 μm × 10 μm was obtained by using the mapping scan mode (Fig. S12). No obvious change in the intensity of the G peak on slid MoS_2 region was around the graphite flake, and all were at the reference value. Further, the Raman characterization results at different positions (points 1-121) on the slid MoS_2 surface are shown in Fig. S12. No observable G peak (1580 cm^{-1}) and defect peak of MoS_2 indicated that there was no visible graphite wear debris and no defect of MoS_2 on the slid MoS_2 surface after 140,000 sliding cycles.

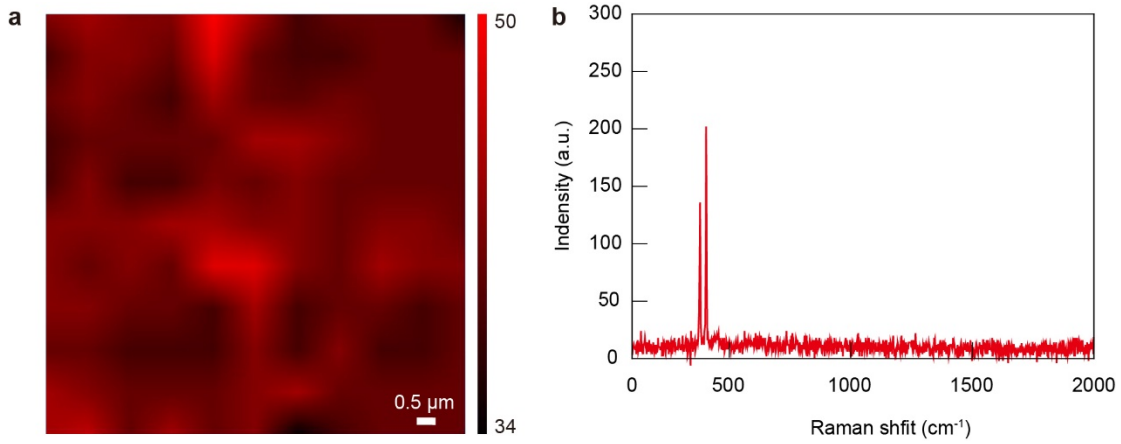

Fig. S12. Raman characterization of slid MoS_2 surface: (a) Intensity distribution of the G peak (1580 cm^{-1}) in the range of 10 μm × 10 μm. (b) Raman characterization results on the slid MoS_2 interface.

S13. Raman mapping of SMGs

Before characterizing the slid graphite flake surface, we first used the method shown in Fig. S13 to lift the graphite flake by overcoming the van der Waals adsorption force

between graphite flake and MoS_2 interfaces. The whole process consists of three steps: In step 1, we placed the AB glue mixed in a ratio of 1:1 on the glass slide and put it in the ambient atmosphere for 30 mins, and then we used a tungsten micro-tip controlled by a micromanipulator (Kleindiek MM3A) to extend into the AB glue (Fig. S13a). There would be a small glue drop (the diameter is around 4 μm) attached to the micro-tip (Fig. S13a) when we pulled out the micro-tip. In step 2, we aligned the micro-tip with small glue to the top of slid graphite flake (Fig. S13b), and then used the micromanipulator to stick the small glue drop with the graphite flake. In step 3, as the small glue drop was solidified and bonded, the bonding force between the small glue drop and the graphite flake was larger than the van der Waals adsorption force between the graphite flake and MoS_2, so we could lift the graphite flake by using the micromanipulator.

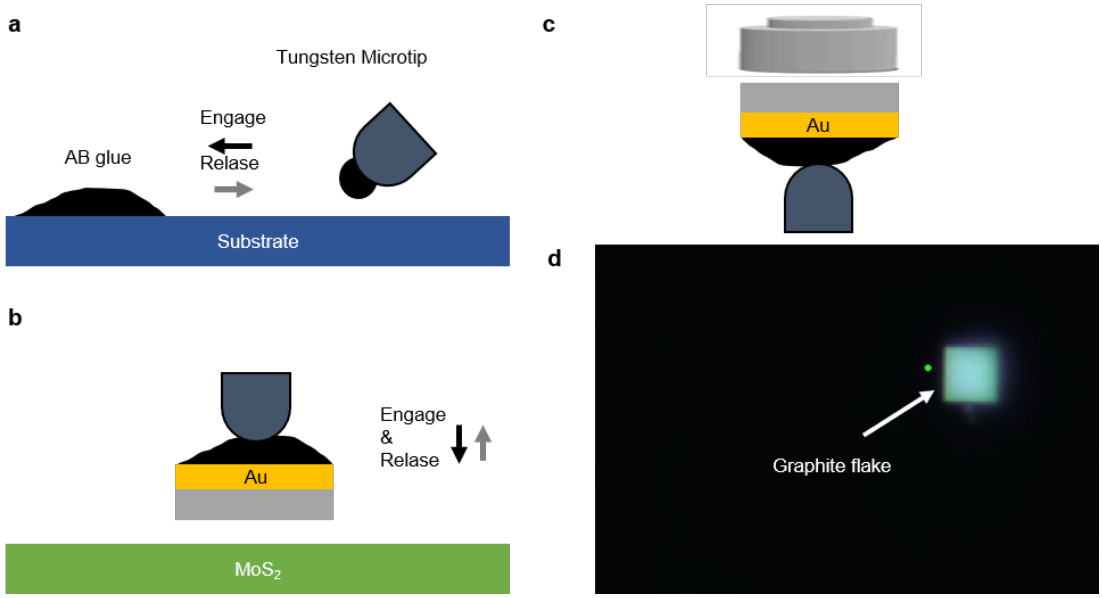

Fig. S13. Methods to stick and flip graphite flakes by using a small glue drop. Step 1: (a) Using a tungsten micro-tip to extend into the AB glue, and pulling out the micro-tip and attach a small glue drop (the diameter is around 4 μm). Step 2: (b) Alignment of micro-tip with small glue drops and graphite flakes. Step 3: Lifting and flipping of the graphite flake from the MoS_2 surface. (c) Turning over the graphite flake. (d) Microscope observation of slid surface of graphite flake.

We then flipped the 180 degrees of the micro-tip to observe the slid surface of the graphite flake by OM (Figs. S13c-d). Furthermore, we performed the Raman characterization on the flipped slid graphite flake interface (Fig. 4d), to judge whether there was any observable damage according to the D peak and the peak of MoS_2 (A^1_g E_{2g}).

S14. Resolution of Raman characterization for defects in graphite

As limited by the equipment, the Raman measurements showed a certain degree of noise. Therefore, we cannot observe D peaks (1350 cm^{-1}) below the noise level. The percentage of defect ρ in graphite can be obtained according to the intensity ratio of D peak (1350 cm^{-1}) and G peak (1580 cm^{-1}), which $\rho = k(I_D/I_G)^2$ where $k = 0.022$. According to the Raman results shown in Fig. 3d, we obtain that the maximum value of I_D/I_G is around 0.03, and the defect density ρ is around 0.002%, which defines the resolution of Raman measurements for defects in graphite.

S15. Transmission line models

In the contact under pressure enforced by the AFM tip, electronic couplings between the graphene and MoS_2 layers create conducting channels for electronic tunneling, whereas other areas are still in the typical Schottky diode contact. The transfer carriers thus will be activated locally. This mechanism can be explained in a circuit model (Fig. S14), in which we use a large contact resistance to represent the Schottky diode. The vertical resistance of the whole system is $(R_{MoS2}\ R_{SHB})^{1/2}$ if there are no conducting channels for the electrons. Once a few conducting channels are activated, the vertical resistance decreases significantly.

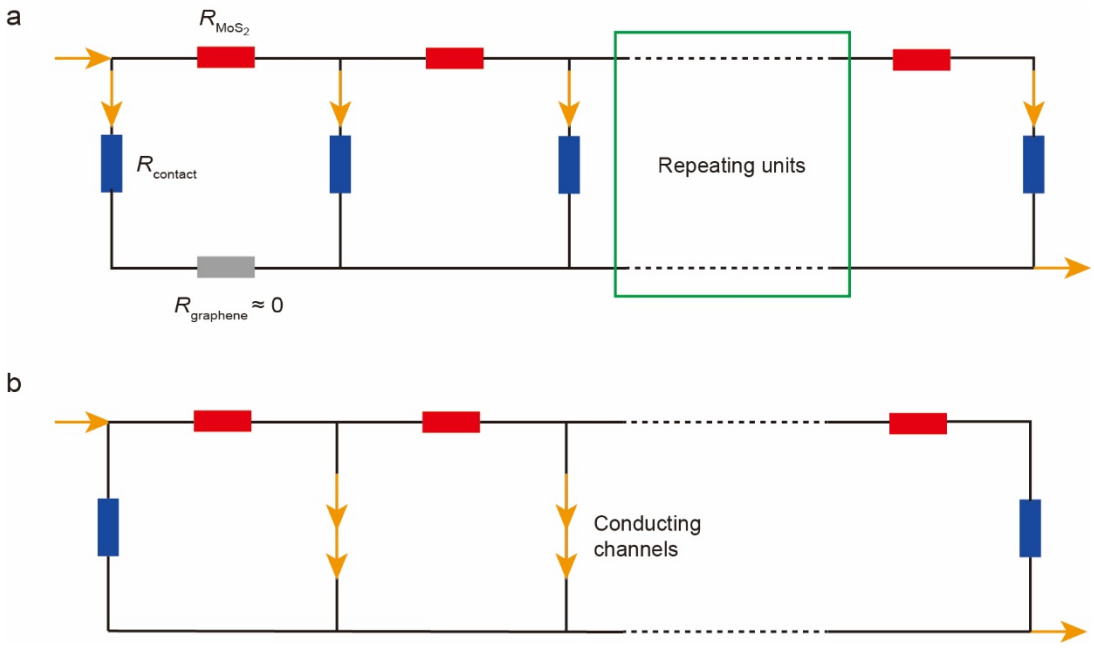

Fig. S14. Schematic diagram of the transmission line model, $R_{contact}$, R_{MoS2}, $R_{graphene}$ the resistance per unit length for the Schottky contact, MoS_2, and graphene respectively. (a) In the absence of pressure, the resistance $R_{contact}$ cannot be neglected for the nature of the Schottky diode. (b) As a few conducting channels are activated under pressure, the contact resistance decreases and the current can flow through the interface.

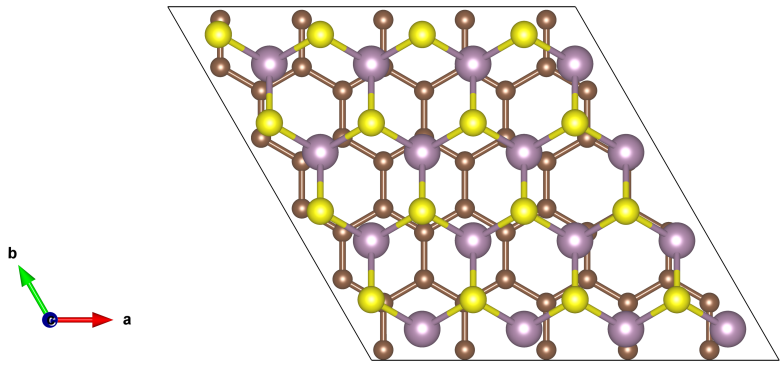

Fig. S15. Structure of the graphene/MoS_2 supercell constructed for first-principles calculations.

Supplementary References

1 Lu, X. K., Yu, M. F., Huang, H. & Ruoff, R. S. Tailoring graphite to achieve single sheets. *Nanotechnology* **10**, 269-272 (1999).

2 Zheng, Q. *et al.* Self-retracting motion of graphite microflakes. *Physical Review Letters* **100**, 067205 (2008).

3 Wang, K., Qu, C., Wang, J., Quan, B. & Zheng, Q. Characterization of a microscale superlubric graphite interface. *Physical Review Letters* **125**, 026101 (2020).

4 Sader, J. E., Chon, J. W. M. & Mulvaney, P. Calibration of rectangular atomic force microscope cantilevers. *Review of Scientific Instruments* **70**, 3967-3969 (1999).

5 Sader, J. E., Larson, I., Mulvaney, P. & White, L. R. Method for the calibration of atomic-force microscope cantilevers. *Review of Scientific Instruments* **66**, 3789-3798 (1995).

6 Li, Q., Kim, K. S. & Rydberg, A. Lateral force calibration of an atomic force microscope with a diamagnetic levitation spring system. *Review of Scientific Instruments* **77**, 2209953 (2006).